Temperature dependence of rate coefficients for the gas phase reaction of OH with 3-chloropropene. A theoretical and experimental study

Mariela Aguilera Sammaritano, Mauro González Vera, Pablo Marcelo Cometto, Tatiane Nicola Tejero, Glauco F. Bauerfeldt, Abdelwahid S Mellouki

Temperature dependence of rate coefficients for the gas phase reaction of OH with 3-chloropropene. A theoretical and experimental study.

Mariela Aguilera Sammaritano[1], Mauro González Vera[1], Pablo Marcelo Cometto[*1], Tatiane Nicola Tejero[2], Glauco F. Bauerfeldt[2], Abdelwahid Mellouki[3]

[1] CONICET. Instituto de Altos Estudios Espaciales "Mario Gulich". UNC-CONAE. Falda del Cañete. Ruta provincial 45 km 8. Córdoba. Argentina.

[2] Departamento de Química Fundamental. Instituto de Química. Universidade Federal Rural do Rio de Janeiro. Rodovia BR 465, km 49. Seropédica, RJ. Brazil.

[3] Institut de Combustion, Aérothermique, Réactivité et Environnement (ICARE), CNRS, 1C avenue de la Recherche Scientifique, 45071 Orléans Cedex 02, France

Keywords: allyl chloride, OH radical, gas phase reaction, PLP-LIF, theoretical calculations

Corresponding Authors

e-mail: pablocometto@gmail.com Tel: +54 9 3547 400000 int. 1164

Credit Author Statement

Mariela Aguilera Sammaritano: investigation, formal analysis, visualization, writing (review). **Mauro González Vera:** investigation, formal analysis. **Pablo Cometto:** conceptualization, investigation, formal analysis, writing (original draft, review & editing), resources, funding acquisition and supervision. **Tatiane Nicola Tejero:** investigation. **Glauco Bauerfeldt:** software, resources, formal analysis, writing (review), supervision. **Abdelwahid Mellouki:** resources, formal analysis, funding acquisition, writing (review), supervision.

Abstract

This work studies the mechanism steps of the OH radical + 3-chloropropene gas phase reaction that could explain the apparent negative activation energy experimentally observed. A reinvestigation of the rate coefficients (*k*) temperature dependence, using a PLP-LIF technique, between 253 and 371 K, was performed to provide new data for kinetic parameters critical revisions. A canonical Variational Transition State Theory study was performed to obtain the *k* temperature dependence considering four additions and one H atom abstraction pathways. The theoretical results can explain the experimental Arrhenius behavior, being an OH addition channel not described in previous literature the main reaction pathway.

1. Introduction.

3-Chloropropene is an important intermediate in the petrochemical industry that is used to synthesize epichlorohydrin and glycerin, allyl compounds such as allyl alcohol, allyl amines, allyl esters, and polyesters[1]. Its derivatives are found in varnishes, plastics, adhesives, perfumes, pharmaceuticals, and insecticides[2]. U.S. Environmental Protection Agency (EPA) considers 3-Chloropropene to be a possible human carcinogen[3] and that individuals may be exposed through breathing contaminated air[2].

Its atmospheric chemistry has been investigated by various groups, Albaladejo et al. [4] have concluded that the gas phase reaction with OH radical constitutes its main atmospheric removal process in the troposphere. Grosjean[5] has proposed that the reaction releases Cl atoms and leads to carbonyl compounds as reported by Zhang et al.[6] and Tuazon et al.[7]

To the best of our knowledge, the reaction of OH with 3-chloropropene has been investigated by a limited number of groups. Edney et al.[8, 9] and Tuazon et al.[7] used the relative rate method to determine the rate coefficient value at room temperature in N_2 as bath gas. Martinez et al.[10] have estimated k_{298K} by the relationship between the rate coefficients of the reactions of the OH and NO_3 radical with a haloprenes series. The only absolute measurement was performed by Albaladejo et al.[4] in the temperature range 228 - 388 K, using the pulsed laser photolysis-laser induced fluorescence technique (PLP-LIF) with He as carrier gas.

$OH + CH_2=CHCH_2Cl \rightarrow$ products $\qquad k \qquad$ [1]

k refers to the second order rate coefficient for the global reaction (that will be under scripted *as* $k_{\text{-}cVTST}$, when is theoretically calculated in this work). The temperature dependence of *k* shows slight negative activation energy. This behavior is widely observed in the gas phase reaction of OH radical with unsaturated volatile organic compounds (UVOCs)[11-13]. In general, the negative dependence of the rate coefficients with the temperature has been justified by a mechanism in which the reversible formation of a pre-barrier complex takes place in the OH radical electrophylic addition to the double bond, followed by an irreversible reaction step through a saddle point, to products.[14-16]. In particular, Zhang et al.[6] have computationally investigated the gas phase reaction of OH radical with 3-Chloropropene to products at 100 Torr and between 200–600 K temperature range. They have considered two addition and four hydrogen abstraction pathways. They have employed a variational transition state model and multichannel RRKM theory to calculate the temperature and pressure dependence of the rate constants.

In the present work we have reinvestigated the temperature dependence of *k* using a PLP-LIF apparatus, in order to provide new data for critical revisions of kinetic parameters. In addition, we have conducted a computational study paying special attention to the OH addition channels. To the best of our knowledge, this is the first study that uses a canonical Variational Transition State Theory (cVTST) over four addition and one H atom abstraction pathways to calculate the temperature dependence of *k*.

2. Methodology

2.1. Experimental

The experiments were conducted using the absolute method of PLP-LIF to determine the rate coefficients for the reaction [1] in the temperature range 253-371 K at around 100 Torr.

The PLP-LIF experimental system used is located at the CNRS (Orléans, France). The details of the experimental setup and methodology used have been presented previously[17] . Therefore, the description below is limited to the necessary features to understand the current experiments.

OH radicals were generated by photolysis of H_2O_2 at λ= 248 nm (KrF excimer laser). The concentration of OH radicals was monitored at various reaction times ranging from 10 μs to 10 ms, by pulsed laser induced fluorescence (LIF). A frequency-doubled dye laser pumped by a Nd:YAG laser was used to excite the OH radicals at λ= 282 nm, and fluorescence from OH radicals was detected by a photomultiplier tube fitted with a 309 nm narrow bandpass filter. The output pulse from the photomultiplier was integrated for a preset period by a gated charge integrator. Typically, the fluorescence signal resulting from 100 probe laser shots was measured for 10 to 15 different delay times and averaged to generate OH concentration-time profiles over 2.5 - 3 lifetimes. H_2O_2 was introduced into the reaction cell by passing a small flow of helium through a glass bubbler containing a solution of H_2O_2. 3-chloropropene was premixed with helium in a 10 L glass bulb to form a 0.2-0.4% mixture at total pressure of about 1000 Torr. The gas mixture, the photolytic precursor (H_2O_2), and the bath gas (He) were flowed through the cell with a linear velocity in the range 3-10 cm s^{-1} and the residence time in the cell reaction zone is estimated less than 0.1 s. Each photolysis/probe sequence interrogated a fresh gas mixture, and reaction products did not build up in the cell. The 3-chloropropene concentrations were calculated from their mass flow rates, the temperature and the pressure in the reaction cell. All flow rates were measured with mass flow meters calibrated by measuring the rate of pressure

increase in a known volume. The pressure in the cell was measured with a capacitance manometer connected at the entrance of the cell.

Rate coefficients were determined under pseudo-first-order conditions with the concentration of 3-Chloropropene in excess over that of OH radicals ($[CH_2=CHCH_2Cl]_0 > 10\ [OH]_0$). The rate of disappearance of OH radical followed a simple exponential rate law:

$[OH]_t = [OH]_0\ e^{-k't}$ where $k' = k\ [CH_2=CHCH_2Cl] + k'_0$

Where k represents the second order rate coefficient for the global reaction [1] and k'_0 is the first-order rate coefficient for OH removal in the absence of 3-chloropropene due to the diffusion of OH radicals out of the detection zone (which have a rate coefficient of 30 s^{-1} in the set up) and the reaction between OH radicals and their precursor (H_2O_2).

Experiments were carried out in the temperature range 253-371 K and at total pressure between 101 and 107 Torr of helium. The experimental conditions are summarized in Table 1.

2.3. Materials.

The helium carrier gas (Alpha Gas UHP certified to > 99.9995%). The 50 wt% H_2O_2 solution, from Prolabo, was concentrated by bubbling helium through the solution to remove water for several days prior to use and constantly during the experiment. 3-Chloropropene Aldrich (99%), was degassed by repeated freeze-pump-thaw cycles and purified by vacuum distillation before use.

2.4. Theoretical Calculations

Taking into account the experimental and theoretical results of Tuazon et al.[7] and Zhang et al.[6], we have considered in this work that at temperatures lower than 600 K the rate limiting step of the reaction [1] is determined by a mechanism composed by OH addition to double bond and the β-H atom abstraction parallel reactions, according to the following general scheme:

$CH_2=CHCH_2Cl + OH \rightarrow \sigma\text{-PC}$	(k_1)	[2]
$\sigma\text{-PC} \rightarrow CH_2=CHCH_2Cl + OH$	(k_{-1})	[3]
$\sigma\text{-PC} \rightarrow I_c$	($k_2(c)$)	[4]
$\sigma\text{-PC} \rightarrow I_t$	($k_2(t)$)	[5]
$CH_2=CHCH_2Cl + OH \rightarrow \sigma\text{-PC}_\beta$	(k_3)	[6]
$\sigma\text{-PC}_\beta \rightarrow CH_2=CHCH_2Cl + OH$	(k_{-3})	[7]
$\sigma\text{-PC}_\beta \rightarrow I_{abs} + H_2O$	(k_4)	[8]

where, σ-PC is the pre-barrier complex, I_c and I_t are the products of the OH addition to the central and terminal carbon atoms, σ-PC_β is the pre-barrier complex and I_d is the product of the β-H atom abstraction, and, in parentheses, the k_i (being i= 1, 2, 3, 4, -1 and -3) are the rate coefficients corresponding to each reaction step. k_4 is the rate coefficient for the H abstraction channel.

Reaction [1] (involving the elementary reactions [2-8] and the further splitting explained in the discussion section) has been described at Density Functional Theory (DFT) level, [18] adopting the M06-2X functional[19] along with the aug-cc-pVTZ basis sets [20]. Geometry optimizations aiming to the location of all minima and saddle points have been performed and the characterization of these stationary points, after the converged geometry optimization calculations, has been done by analysis of the vibrational frequencies, calculated at the same level. Also, in order to guarantee that the optimized structure corresponds to a global or local minimum, relaxed scans along one or more dihedral angles have been calculated. This procedure has been adopted because the potential energy surface is expected to show a high density of minima, due to the combination of some internal rotations, differing one from the other by a few kcal mol^{-1}. Theoretical calculations have been performed with the GAUSSIAN09 program packages[21]. The stationary points can be summarized as reactants, pre-barrier complex, saddle point and products. The minimum energy paths connecting the pre-barrier complex and product and passing through the saddle point have been calculated using the intrinsic reaction path (IRC) method[22]. For the description of the minimum energy path connecting the pre-barrier complex and the reactants, scan calculations have been performed by partially optimizing the geometries along a path of increasing C–OH interatomic distances. Thermochemical quantities have been calculated using conventional statistical thermodynamics relations, assuming the harmonic oscillator, rigid rotor and ideal gas models[23]. In this work, we have also carried out single point calculations at the CCSD(T)/aug-cc-PVTZ level based on the M06-2X/ aug-cc-PVTZ optimized geometries, in order to improve the electronic energies. The Zero Point Energy (ZPE) corrections at the CCSD(T)/cc-aug-PVTZ were assumed the same corrections obtained from the vibrational frequencies calculated at the M06-2X/cc-aug-PVTZ level, then, unless otherwise specified, the geometric parameters and energies used in the following discussion is CCSD(T)/cc-aug-PVTZ// M06-2X/aug-cc-PVTZ + ZPE level. All open-shell stationary points showed T1 diagnosis values lower than 0.04 and no multiconfigurational character should be expected.

Canonical Variational Transition State rate coefficients have been calculated using the model described elsewhere[24]. Briefly, the minimum energy path, described by the total energy as a function of the reaction coordinate (s) and suggested from IRC or scan calculations, is transformed into a vibrationally adiabatic potential energy curve by including the zero-point energy corrections of the non-stationary points that define the reaction path. A further transformation into a Gibbs free energy curve, G(s,T), at each temperature, is possible with the inclusion of the enthalpy and entropic correction terms provided from the thermodynamics formulations mentioned above. A polynomial of third or fifth order is fitted to the Gibbs free energy curves and the resulting G(s,T) functions are analytically maximized to obtain the s values that correspond to the location of the generalized transition state at each temperature. Molecular properties (vibrational frequencies, moments of inertia and critical energy) of the generalized transition states are interpolated and applied as the input quantities for the conventional Eyring equation[25] over the temperature range 200–400 K.Tunneling coefficients were calculated using the Wigner's expression[26].

Since formation of the prebarrier complexes are barrierless reaction paths, conventional transition state method does not apply for the prediction of the rate coefficients. Moreover, entropy effects are important for the best evaluation of rate coefficients of reaction that proceed through relatively small barrier heights. For these reasons, the adoption of the canonical variational method for predicting rate coefficients is crucial.

3. Results and discussion

3.1. Experimental

The absolute rate coefficients were measured in the temperature and pressure ranges 253 - 371 K and 101-104 Torr (of helium) under pseudo-first-order conditions in which the concentration of the 3-Chloropropene was at least 10 times than OH radicals' concentration. The OH decays were found to be exponential over at between 2.5 and 3 lifetimes while k'_0 and k' were in the ranges 212-617 s^{-1} and 552-2875 s^{-1}, respectively. The variation of the photolysis fluence (7.7-21 mJ cm^{-2}) had no effect on the determined rate coefficient indicating that there was no noticeable contribution of photofragments to the OH consumption. The CH_2=$CHCH_2Cl$ samples were purified to better than 99% and hence loss of OH radicals by reaction with impurities is expected to be insignificant.

Figure 1.a. shows an example of pseudo-first-order plots for the OH radical signal decay and in Fig 2.b., as an example, a plot of (k'-k'_0) as a function of CH_2=$CHCH_2Cl$ concentration at different temperatures, is presented. The k values obtained in this

work at different temperatures are shown in Table 1, related to experimental conditions. The rate coefficient, taken as the average of all values obtained at 298 ± 2 K was

$$k = (1.69 \pm 0.12) \times 10^{-11} \text{ cm}^3 \text{ molecule}^{-1} \text{ s}^{-1}$$

The errors quoted for *k is* 2σ from the linear least-squares fit to the data points and do not include systematic errors. This value is in good agreement with those obtained by other authors[4, 6, 7- 9] using different techniques, which are presented in Table 2. There is no significant difference between the *k* value, obtained in this work at 298 K and a pressure of 100 Torr, and the value of $(1.64\pm0.18)\times10^{-11}$ cm^3 molecule^{-1} s^{-1}obtained in similar experimental conditions by Albaladejo et al.[4], and the values of $(1.66\pm0.23)\times10^{-11}$ $(1.70\pm0.70)\times10^{-11}$, $(1.96\pm0.32)\times10^{-11}$and $(1.69\pm0.07)\times10^{-11}$, (in units of cm^3 molecule^{-1} s^{-1}), obtained by Albaladejo et al.[4], Edney et al.[8, 9] and Tuazon et al.[7], respectively, at 298 K and 1 atm. Thus, our results confirm that at 100 Torr *k* is in its high-pressure limit. All these values are presented in the inset of the Figure 2.

Figure 2 show the measured rate coefficients for the studied reaction plotted as a function of the reciprocal of temperature along with *k* obtained in this work. A least-squares analysis of the ln *k* versus 1/T plot leads to the following expression for the temperature dependence of *k*, in the temperature range 253-371 K (in units of cm^3 molecule^{-1} s^{-1}):

$$k = (2.82 \pm 0.38) \times 10^{-12} \exp\{(540 \pm 42) / T\}$$

Uncertainties are 2 σ_{lnA} and 2 $\sigma_{E/R}$ for A and E/R, respectively.

Table 2 presents theoretical and experimental rate coefficients temperature dependence for the global reaction [1] determined previously by other authors[4, 6]. The results show negative temperature dependence for *k* in agreement with the Albaladejo et al.[4] work. This fact is consistent with the hypothesis that the addition mechanism is the main reaction pathway in the considered temperature range.

3.2. Theoretical Calculations

We begin our discussion by investigating the CH_2=$CHCH_2Cl$ potential energy surface aiming to explore the possible rotamers of the reactant and the location of the minimum energy geometry. Therefore, scan calculations over the dihedral angles were performed at the M06-2X/aug-cc-pVTZlevel. Possible rotamers can arise from the rotation of the -CH_2Cl group. Three minima were found, one of them correspond to the structure CH_2=$CHCH_2Cl$–C_s (rotamer belonging to the C_s symmetry group), shown in the Figure 3, the other minima are mirror images belonging to the C_1 symmetry group, and have the structure shown in the same Figure labeled as CH_2=$CHCH_2Cl$–C_1. CH_2=$CHCH_2Cl$–Cs lies 0.49 kcal mol^{-1} above the CH_2=$CHCH_2Cl$–C_1 rotamer and the

barrier height separating them is 2.47 kcal mol^{-1}, as predicted at the M06-2X/aug-cc-pVTZ level. Reactions of each rotamer were treated individually. After the location of the possible rotamers, from the scan calculations, the energy was corrected at the CCSD(T)/aug-cc-pVTZ level.

The finding of the CH_2=$CHCH_2Cl$–C_s and CH_2=$CHCH_2Cl$–C_1 rotamers suggests that the OH radical can attack in two different ways. The first one is from the upside of the plane defined by the three C atoms, *i.e.*, from the same side where the Cl atom is located, hereafter referred as the upward attack. The second way is given if the OH attack is from the opposite side of that plane, thus, a downward attack is proposed. For the CH_2=$CHCH_2Cl$–C_1 rotamers only the downward attack leads to a sigma pre-barrier complex (σ-PC_{down}) connected by $TS_{c\text{-}down}$ and $TS_{t\text{-}down}$ to $I_{c\text{-}down}$ and $I_{t\text{-}down}$, whose geometries are also shown in Figure 3. The subscripted c-down and t-down denote the downward addition pathways to the central and the terminal carbon atoms of the double bound of the CH_2=$CHCH_2Cl$–C_1, respectively. In the Figure 4a-b, the geometries of 2 stereoisomers of the σ-PC_{down} (energetically degenerated) are shown. As far as we know, this work provides the first description of these OH addition pathways for the reaction [1].

On the other hand, in the CH_2=$CHCH_2Cl$–C_s rotamer the chlorine atom lies in the same plane defined by the three C atoms, as can be observed in Figure 3. During the OH radical attack, the Cl atom takes place over the plane at the same side of the OH (forming an 8º dihedral angle between the plane and the C-Cl bond), to form the σ-PC_{up} connected by $TS_{c\text{-}up}$ and $TS_{t\text{-}up}$ to $I_{c\text{-}up}$ and $I_{t\text{-}up}$. Accordingly, the subscripted c-up and t-up denote the upward addition pathways to the central and the terminal carbon of the double bound of the CH_2ClCH=CH_2 –C_s, respectively. All these structures are shown in Figure 3. In the upward OH attack 2 σ-PC_{up} stereo-isomers can be formed, which are energetically degenerated. The geometries for those isomers are shown in Figure 4c-d. Then, two parallel reaction pathways (one for each stereo-isomer) for the upward OH addition have been considered. Along the upward reaction channel, we have found molecular structures similar to the CR1, TS1, TS2, IM1 and IM2 proposed by Zhang et al.[6] for the OH addition to CH_2ClCH=CH_2.

Summarizing, as a consequence of the presence of the σ-PC_{down} and the σ-PC_{up}, the reactions [2]-[5] are splitted, and the ractions 6-8 are reformulated as follows:

CH_2=$CHCH_2Cl$-C_1 + OH → σ-PC_{down} ($k_{1\text{-}down}$) [2a]

σ-PC_{down} → CH_2=$CHCH_2Cl$-C_1 + OH ($k_{-1\text{-}down}$) [3a]

σ-PC_{down} → $I_{c\text{-}down}$ ($k_{2c\text{-}down}$) [4a]

σ-PC_{down} → $I_{t\text{-}down}$ ($k_{2t\text{-}down}$) [5a]

CH_2=$CHCH_2Cl$-C_s + OH → σ-PC_{up} ($k_{1\text{-}up}$) [2b]

$\sigma\text{-}PC_{up} \rightarrow CH_2{=}CHCH_2Cl\text{-}C_s + OH$ ($k_{1\text{-}up}$) [3b]

$\sigma\text{-}PC_{up} \rightarrow I_{c\text{-}up}$ ($k_{2c\text{-}up}$) [4b]

$\sigma\text{-}PC_{up} \rightarrow I_{t\text{-}up}$ ($k_{2t\text{-}up}$) [5b]

$CH_2{=}CHCH_2Cl\text{-}C_1 + OH \rightarrow \sigma\text{-}PC_{\beta}$ (k_3) [6c]

$\sigma\text{-}PC_{\beta} \rightarrow CH_2{=}CHCH_2Cl\text{-}C_1 + OH$ (k_{-3}) [7c]

$\sigma\text{-}PC_{\beta} \rightarrow I_{abs} + H_2O$ (k_4) [8c]

Regarding on the β-H atom abstraction channel, in this work only the $CH_2{=}CHCH_2Cl$–C_1 rotamer was considered because it is the most stable one and presents two specular structures. A $\sigma\text{-}PC_{\beta}$ connecting reagents to the I_d via the $TS_{\beta\text{-}H}$ was found, which presents two energetically degenerated stereoisomers. The molecular structures are, also, shown in the Figures 4e-f. The $CH_2ClCH{=}CH_2$ –C_1 rotamer belongs to the C_1 symmetry group, thus in the β position the two H atoms are not equivalent. The $TS_{\beta\text{-}H}$ was found only when the OH attack was on the H atom located below the plane of the three carbon atoms. At the considered temperature the abstraction pathways are expected to be minority[6]. Then, in order to study alternative reactions channels to those presented by Zhang et al.[6] in this paper we have just focused beta H abstraction.

The molecular properties (including optimized geometries and frequencies) for all the stationary points, shown in Figure 3, obtained at the CCSD(T)/ aug-cc-PVTZ// M06-2X/ aug-cc-PVTZ level, are given as Supporting Information.

The Table 3 summarizes the relative energy (with respect to the isolated Reactants), expressed in kcal mol^{-1}, for the stationary points along the described reaction pathways. At the M06-2X/aug-cc-PVTZ level the S^2 values were lower than 0.78, then, regarding to the spin contamination, the wave function and electronic energies are not affected by states of higher multiplicity. No calculations with different basis set were carried out because Zhang et al.[6] have obtained ΔE values comparable to the obtained in this work for the species $\sigma\text{-}PC_{up}$, $TS_{c\text{-}up}$, $TS_{t\text{-}up}$, $I_{c\text{-}up}$ and $I_{t\text{-}up}$, at the CCSD(T)/cc-PVTZ//M06-2x/6-311++G(d,p)) level. Also, they have not found dependency of the basis sets in the results.

A description of the potential energy surface for the four addition reactions channels and the β - H atom abstraction pathway is provided in the Figure 5 (and Table 3) and as can be observed, the pre-complexes present ΔE ranging between -3.30 and -4.09 kcal mol^{-1}. The $TS_{c\text{-}down}$, $TS_{t\text{-}down}$, $TS_{c\text{-}up}$ and $TS_{t\text{-}up}$ present negative ΔE ranging between -1.07 and -1.80 kcal mol^{-1}, *i.e.*, below reactants. $TS_{\beta\text{-}H}$ has a ΔE of 0.19 kcal mol^{-1}, over the reactants.

Starting from each saddle point, IRC calculations were performed for the description of the reaction profiles leading to the formation of the chlorinated hydroxy

radicals resulting from the addition of the hydroxyl radical to either the central or the terminal carbon atoms, from upward and downward attacks: $I_{c\text{-}down}$, $I_{t\text{-}down}$, $I_{c\text{-}up}$ and $I_{t\text{-}up}$. On the side, in the β-H atom abstraction channel, the IRC confirmed the reaction path from σ - PC_β to the I_d radical.

For the OH addition to the double bond reactions, π pre-barrier complexes have been proposed in previous studies[14-16, 25], in which the OH radical moiety lies nearly perpendicular to the C=C plane. Such pre complexes were not found in the present work at the level of theory used.

Regarding the reactions pathways, the rate coefficients were calculated for the association step and dissociation and addition reactions of the PC, represented in the reactions 2a-5a, 2b-5b and 6c-8c.

The canonical variational transition state method was adopted using the theoretical molecular properties calculated at M062X level with both and aug-cc-pVTZ basis sets. For the prediction of the global rate coefficients, the mechanism described by the chemical steps 2a-5a, 2b-5b (addition channels) and CH_2=$CHCH_2Cl$-C_1 + OH → σ-PC_β (6c); σ-PC_β → CH_2=$CHCH_2Cl$-C_1 + OH (7c); σ-PC_β →I_β (8c) was assumed. The steady state is assumed for each PC in this mechanism (ie. d[σ-PC_{down}]/dt = d[σ-PC_{up}]/dt = d[σ-PC_β]/dt = 0), and following expressions are obtained for k_{down}, k_{up} and k_{abs} and k_{cVTST} (which is equal to the sum k_{down} + k_{up} + k_{abs}):

$$k_{down} = 2\frac{k_{1-down} \times (k_{2c-down} + k_{2t-down})}{k_{-1-down} + k_{2c-down} + k_{2t-down}} \qquad \text{Eq. 1}$$

$$k_{up} = 2\frac{k_{1-up} \times (k_{2c-up} + k_{2t-up})}{k_{-1-up} + k_{2c-up} + k_{2t-up}} \qquad \text{Eq. 2}$$

$$k_{abs} = 2\frac{k_{1-abs} \times (k_{2-abs} + k_{2-abs})}{k_{-1\,abs} + k_{2-abs} + k_{2-abs}} \qquad \text{Eq. 3}$$

$$k_{-cVTST} = (k_{down} + k_{up} + k_{abs}) \qquad \text{Eq. 4}$$

The factor 2 in the Eq. 1-3 accounts for the degeneracy of the 3 reaction paths (addition -up and down- and abstraction) due to stereochemistry. Tunneling corrections do not apply for the barrierless addition but can slightly increase $k_{2c\text{-}down}$, $k_{2t\text{-}down}$, $k_{2c\text{-}up}$,

$k_{2t\text{-}up}$ and k_4 values. For the hydrogen abstraction channel, the tunneling coefficients ranged from 2.46 to 1.36, as the temperature increases from 200 to 400 K, whereas a range from 1.41 to 1.06 was observed for the Wigner coefficients related to the addition channels. The Table 4 summarizes the results for k_{down}, k_{up}, k_{abs} and $k_{\text{-}cVTST}$ (in this work, predicted using the cVTST method) between 200 and 400 K. These values were plotted in the Figure 2 along with the Arrhenius plot obtained in this work and experimental and theoretical rate coefficient values in previous literature.

The obtained Arrhenius equationis:

$k_{cVTST} = (1.54 \pm 0.08) \times 10^{-12} \exp[(532 \pm 18) / T]$, 275 – 400 K

where k_{cVTST} is the expression obtained by fitting the rate coefficients between 275 – 400 K. Linearity of the classical Arrhenius expression is lost with the extension of the temperature range from 200 – 400 K and the rate coefficients are better fitted by:

$k_{cVTST} = (3.01 \pm 1.21) \times 10^{-19} [T^{(2.27 \pm 0.06)}] \exp[(1284 \pm 16) / T]$, 200 – 400 K

The quoted uncertainties in the equations above were obtained by evaluation he standard errors of regression, at 95% of confidence level.

In agreement with the previous literature concerning the OH addition to unsaturated compounds, addition is the dominant channel at this range of temperatures and shows negative temperature dependence. As is shown in the Table 4 and Figure 2, the H abstraction pathway present positive activation energy and the k_{abs} values are, at least, one order of magnitude lower than the values of k_{down} and k_{up}, at the same temperature. Then, other less important abstraction channels studied by Zhang et al. [6] can be neglected in the $k_{\text{-}cVTST}$ calculation.

The $k_{\text{-}cVTST}$ value at 298 K of 9.13×10^{-12} cm^3 $molecule^{-1}$ s^{-1}reach the 54% and the 59% of the values $(1.69 \pm 0.12) \times 10^{-11}$ and 1.56×10^{-11}(in unit of cm^3 $molecule^{-1}$ s^{-1}), experimentally obtained in this work and calculated by Zhang et al. [6], respectively.

The rate coefficients predicted from the canonical variational transition state method, employed in this work, are underestimated by factors ranging from 1.4 – 2.0 (200 – 400 K). In particular, the room temperature rate coefficient is underestimated by a factor of 1.9. Calculated rate coefficients are also lower than those predicted by Zhang and coworkers, who adopted a microcanonical method, based on the RRKM model, for the calculation of the rate expression. A comparison among canonical and microcanonical rate coefficients for OH reactions with unsaturated compounds can be found elsewhere[15, 16].

Although the rate coefficients have been underestimated with respect the experimental and literature values, the predicted global activation energy agrees very well with the experimental value (-1.06 kcal mol^{-1}, in comparison with -1.07 kcal.mol^{-1},

405 respectively, calculated from 275 – 400 K). The ratio between the calculated and the
406 experimental activation energies between 275 and 400 k is 0.99, which represent a
407 good agreement taking into account the two different employed methods. Our
408 calculations show negative temperature dependence for $k_{,}$ in accordance with the
409 experimental results of Albaladejo et al.[4] This behavior is also predicted by theoretical
410 calculations by Zhang et al.[6] At the same range, the activation energy calculated for the
411 rate coefficients reported by Zhang and coworkers is -1.48 kcal mol^{-1}.

412 The deviation of the cVTST rate coefficients from the experimental values mostly
413 arise from the entropic term in the Eyring expression, which is governed by the values
414 of the lowest vibrational frequencies. Considering the errors in the theoretical prediction
415 of all these parameters, the agreement between predicted and experimental rate
416 coefficients must be considered very good.
417

418 **Conclusions**

419 There is only one previous study of the rate coefficient temperature dependence
420 which is not enough for recommendation in critical revisions, then, this work provides
421 new valuable experimental data of kinetic parameters of the title reaction.

422 As far as we know, this is the first study that uses a cVTST to obtain the
423 temperature dependence of the *k* of the reaction [1] considering four additions and one
424 H atom abstraction pathways.

425 The ratio between the calculated and the experimental activation energies
426 indicates a good agreement between experimental and theoretical results, then,
427 although the calculation of cVTST may underestimate the values of rate coefficients,
428 considering its simplicity, it could be used as an alternative method to describe the
429 temperature dependence for the reactions of haloalkenes with the OH radical.

430 The negative temperature dependence of k_{exp} and $k_{\text{-}cVTST}$ (the last one obtained
431 considering the proposed global mechanism described in the reactions 2a-5b and 6c-
432 8c) could explain the experimental results, and supports the hypothesis that the OH
433 radical addition is the main reaction mechanism for the studied global reaction, being
434 the downward addition the most important reaction channel in the considered
435 temperature range. To the best of our knowledge these not negligible reaction
436 channels have been considered for the first time in this work in order to calculate the
437 temperature rate constant dependence for the global reaction.

438 As a perspective of the ongoing research, a future study on the effects of the DFT
439 method and basis sets over the computational capability to found the π or σ pre-

complexes could be studied. Also, a further study on the impact of the kind of pre-complexes on the cVTST rate coefficient calculations is previewed to be carried out.

Acknowledgments

We thank CONICET, ANPCyT-FONCyT (PICT2016-0698) from Argentina, CNPq from Brazil, and CNRS and ECOS from France and the EU for financial support of this research and for doctoral and posdoctoral fellowships.

References

1- Ullmann`s Fine Chemicals. Wiley-VCH. Verlag Gmbh& Co. Hamburg, Germany. 2014.

2- U.S. Environmental Protection Agency. Health and Environmental Effects Profile for Allyl Chloride. Environmental Criteria and Assessment Office, Office of Health and Environmental Assessment, Office of Research and Development, Cincinnati, OH. 1986.

3- U.S. Environmental Protection Agency. Integrated Risk Information System (IRIS) on Allyl Chloride. National Center for Environmental Assessment, Office of Research and Development, Washington, DC. 1999.

4- J. Albaladejo, B. Ballesteros, E. Jiménez, Y. Díaz de Mera, E. Martínez *Atmos. Environ*. 37 (2003) 2919–2926.

5- D. Grosjean (1991) *J. Air Waste Manage. Assoc.*, 41:2, 182-189.

6- Y. Zhang, K. Chao, J. Sun, W. Zhang, H. Shi, C. Yao, Z.Su, X. Pan, J. Zhang, and R. Wang. *J. Chem. Phys.* 140 (2014), 084309.

7- E.C.Tuazon, R.Atkinson, S.M. Aschmann. *Int. J. Chem. Kinet.* 22 (1990), 981–998.

8- E. O. Edney, P. B. Shepson,T. E. Kleindienst, E. W. Corse. *Int. J. Chem. Kinet.* 18 (1986), 597–608.

9- Edney, E.O., Kleindienst, T.E., Corse, E.W., 1986. *Int. J. Chem. Kinet.*18, 1355–1371.

10- E. Martínez, B. Cabañas, A. Aranda, P. Martín, R. P Wayne. *Journal of the Chemical Society-Faraday Transactions.* 92 (1996), 4385–4389.

11- R. Atkinson, J. Arey, *Chem. Rev.*, 103 (2003), 4605−4638.

12- P. Cometto, Pablo Dalmasso, R. Taccone, S. Lane, A. Mellouki, F Oussar, V. Daële, G. Le Bras. *J. Phys. Chem. A.*112 (2008), 4444-4450.

13- P. Cometto, V. Daële, M. Idir, S. Lane, A.Mellouki. *J. Phys. Chem. A.*113 (2009), 10745-10752.

14- J. Abbatt, J. Anderson. *J. Phys. Chem.*, 95 (1991), 2382- 2390.

15- T. Da silva barbosa, J. Nieto, P. Cometto, S. Lane, G. Bauerfeldt, G. Arbilla. *RSC adv.* 4 (2014), 20830-20840.

16- S. Peirone, J. Nieto, P. Cometto, T. Da Silva Barbosa, G. Bauerfeldt, G. Arbilla, S. Lane. *J. Phys. Chem. A*. 119 (2015), 3171–3180.

17- A. Mellouki, S. Téton, G. Le Bras. *Int. J. Chem. Kinet.* 27(1995), 791- 805.

18- I. Levine, Quantum Chemistry, Prentice Hall, New Jersey, 2000.

19- A. D. Becke, *J. Chem. Phys.*, 98 (1993), 1372 - 1377.

20- T. H. Dunning.*J. Chem. Phys.* 90 (1989), 1007 - 1023.

21- M. Frisch, G. Trucks, H. Schlegel, G. Scuseria, M. Robb, J. Cheeseman, G. Scalmani, V. Barone, B. Mennucci, G. Petersson, H. Nakatsuji, M. Caricato, X. Li, H. Hratchian, A. Izmaylov, J. Blondo, G. Zheng, J. Sonnenberg, M. Hada, M. Ehara, K. Toyota, R. Fukuda, J. Hadsegawa, M. Ishida, T. Nakajima, Y. Honda, O. Kitao, H. Nakai, T. Vreven, J. Montgomery Jr, J. Peralta, F. Ogliaro, M. Bearpark, J. Heyd, E. Brothers, K. Kund, V. Staroverov, R. Kobayashi, J. Normand, K. Raghavachari, A. Rendell, J. Burant, S. Iyengar, J. Tomasi, M. Cossi, N. Rega, J. Millam, M. Klene, J. Knox, J. Cross, V. Bakken, C. Adamo, J. Jaramillo, R. Gomperts, R. Stratmann, O. Yazyev, A. Austin, R. Cammi,C. Pomelli, J. Ochterski, R. Martin, K. Morokuma, V. Zakrzewski, G. Voth, P. Salvador, J. Dannenberg, Farkas, J. Foresman, S. Dapprich, A. Daniels, O. Ortiz, J. Cioslowski, D. J. Fox, Gaussian09, (RevisionA.02), Gaussian, Inc., Wallingford, CT, 2009.

22- K. Fukui, *J. Phys. Chem.* 74 (1970), 4161 - 4163.

23- P. Ayala, H. Schlegel. *J. Chem. Phys*. 108 (1998), 2314 - 2325.

24- R. Oliveira, G. F. Bauerfeldt. *Int. J. Quantum Chem.* 112 (2012), 3132 - 3140.

25- I. Díaz-Acosta, J. Alvarez-Idaboy, A. Vivier-Bunge. *Int. J. Chem Kinet*: 31 (1999), 29–36.

26. C. J. Cramer. Essentials of Computational Chemistry Theories and Models. John Wiley and Sons, New York, 2004.

507 **Table 1:** Summary of experimental conditions and results for measurements of the rate

T (K)	P (torr)	f ♣	[OH] / (10^{11})[a]	[H_2O_2] / (10^{14})[a]	[$CH_2ClCH=CCH_2$] / (10^{13})[a]	k'_0 (s^{-1})	k' (s^{-1})	$k \pm 2\sigma$ / (10^{-11})[b]
253	102-103	8.4	6.3	3.4	2.00-9.15	525-617	1028-2782	2.49±0.16
273	102-103	8.4	6.2	3.3	2.33-9.40	532-592	1053-2523	2.16±0.10
273	102-103	7.7	5.9	3.4	1.61-6.29	550-610	973-1949	2.15±0.15
298	101-103	21.0	13.2	2.9	1.42-14.67	473-517	713-2875	1.63±0.05
298	102-104	9.1	6.3	3.1	2.23-10.66	497-565	965-2471	1.78±0.12
298	102-104	7.7	7.7	4.3	1.87-8.29	861-601	886-1954	1.67±0.08
323	101-103	11.2	4.9	2.2	2.08-16.19	337-405	680-2828	1.54±0.07
347	102-104	11.2	5.2	2.3	2.72-18.48	356-416	800-2741	1.33±0.06
370	101-103	9.8	2.6	1.5	2.52-19.60	212-308	552-2620	1.21±0.08
371	101-104	9.8	4.0	2.1	2.33-18.18	326-378	651-2649	1.26±0.05

508 coefficient of the gas phase reaction between OH and $CH_2ClCH=CCH_2$.

509 [a] molecule cm^{-3}

510 [b] cm^3 molecule $^{-1}$ s^{-1}

511 ♣Laser Pulse Fluency. mJ cm^{-2}

512

513 **Table 2:**Summary of previous experimental and theoretical values obtained for k_{global} in
514 the high-pressure limit between 253 K and 371 K.

515

Temperature (K)	*k** Ref. 4	*k** Ref. 8	*k** Ref. 9	*k** Ref. 7	*k** Ref.10	*k**[a] Ref.6
228	2.64±0.40					3.51
253	2.41±0.32					2.49
273	2.05±0.28					1.98
296	1.66±0.23					1.59
298	1.64±0.18	1.70±0.70	1.96±0.32	1.69±0.07	1.53±0.40	1.56
323						1.28
328	1.48±0.25					1.24
347						1.10
370						0.960
371						0.955
388	1.18±0.20					0.877

516 * All the values are in units of cm^3 $molecule^{-1}$ $s^{-1}$and were multiplied by $1x10^{11}$.

517 [a] The values were calculated using the expression $k= 2.64 \times 10^{-14} \times T^{0.57} \times \exp$
518 (934.47/T) for the high-pressure limit and the 200-500K temperature range. Ref. 6 the *k*
519 values were theoretically calculated.

520

521

Table 3: Summary of the relative energy (with respect to the isolated Reactants), expressed in kcal mol^{-1}, obtained in this work along with comparable values from Ref. 6.

Species	ΔE + ZPE (M06-2X/aug-cc-PVTZ)	ΔE + ZPE* (CCSD(T)/aug-cc-PVTZ)	ΔE + ZPE[a]Ref. 6.
Addition			
$CH_2ClCH=CH_2$ –C_t + OH	0.00	0.00	
σ-PC_{down}	-3,30	-1,90	
$TS_{c\text{-}down}$	-1,28	-1,58	
$TS_{t\text{-}down}$	-1,07	-1,13	
$I_{c\text{-}down}$	-30,44	-27,44	
$I_{t\text{-}down}$	-31,16	-27,51	
$CH_2ClCH=CH_2$ –C_c +OH	0.00	0.00	0.00
σ-PC_{up}	-4,09	-2,49	-3.56
$TS_{c\text{-}up}$	-1,80	-2,05	-1.96
$TS_{t\text{-}up}$	-1,15	-1,28	-1.03
$I_{c\text{-}up}$	-31,84	-28,76	-29.91
$I_{t\text{-}up}$	-31,86	-27,43	-29.86
β-H atom abstraction			
$CH_2ClCH=CH_2$ + OH	0.00	0.00	
σ - PC_{β}	-3,48	-2,41	
$TS_{\beta\text{-}H}$	0,189	0,64	
I_d + H_2O	-33,38	-31,61	

* Zero Point Energy corrections were calculated from the vibrational frequencies obtained at the M06-2X/cc-aug-PVTZ level.

[a](CCSD(T)/cc-PVTZ//M06-2x/6-311++G(d,p))

Table 4: Summary of conditions and results for cVTST calculations of the rate coefficients for the pathways down. up and abstraction and the global reaction.

Temperature (K)	k_{down}	k_{up}	k_{abs}	k_{-cVTST}
200	1.01×10^{-11}	1.98×10^{-11}	6.87×10^{-13}	3.06×10^{-11}
225	7.28×10^{-12}	1.17×10^{-11}	7.36×10^{-13}	1.97×10^{-11}
250	5.65×10^{-12}	7.67×10^{-12}	7.82×10^{-13}	1.41×10^{-11}
275	4.62×10^{-12}	5.50×10^{-12}	8.23×10^{-13}	1.09×10^{-11}
298	4.00×10^{-12}	4.27×10^{-12}	8.62×10^{-13}	9.13×10^{-12}
300	3.96×10^{-12}	4.19×10^{-12}	8.67×10^{-13}	9.01×10^{-12}
325	3.50×10^{-12}	3.39×10^{-12}	9.06×10^{-13}	7.80×10^{-12}
350	3.17×10^{-12}	2.84×10^{-12}	9.52×10^{-13}	6.96×10^{-12}
375	2.93×10^{-12}	2.47×10^{-12}	9.89×10^{-13}	6.39×10^{-12}
400	2.73×10^{-12}	2.18×10^{-12}	1.04×10^{-12}	5.95×10^{-12}

* All the values are in units of cm^3 $molecule^{-1}$ s^{-1}.

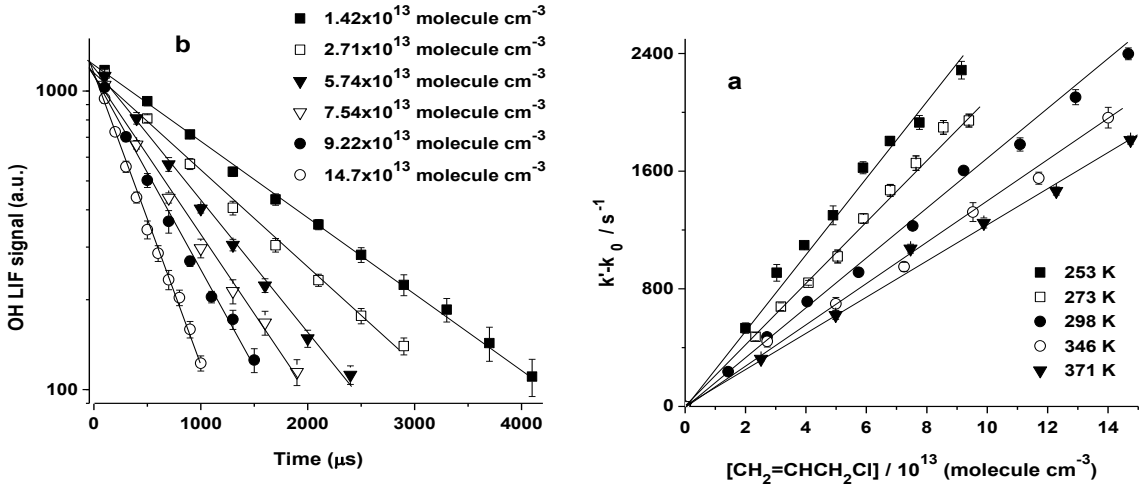

Figure 1: a. Example of pseudo-first-orden plots for the OH radical signal decay at 298 K and four $CH_2ClCH=CH_2$ concentrations. **b.** Examples of plots of the rate of disappearance of the OH radical (k'-k'_0) vs. $CH_2ClCH=CH_2$ concentration at different temperatures.

552

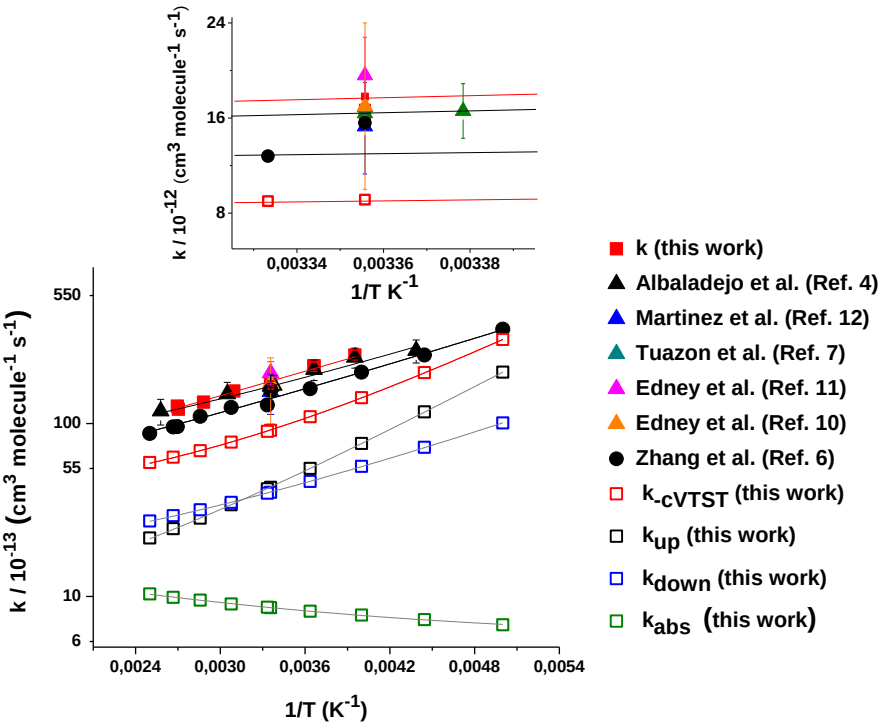

553

554

555 **Figure 2.** Plot of k_1 as function of 1/T for the OH reaction with $CH_2ClCH=CH_2$ in the
556 temperature range 263-369 K, compared with previous results in literature.

557

558

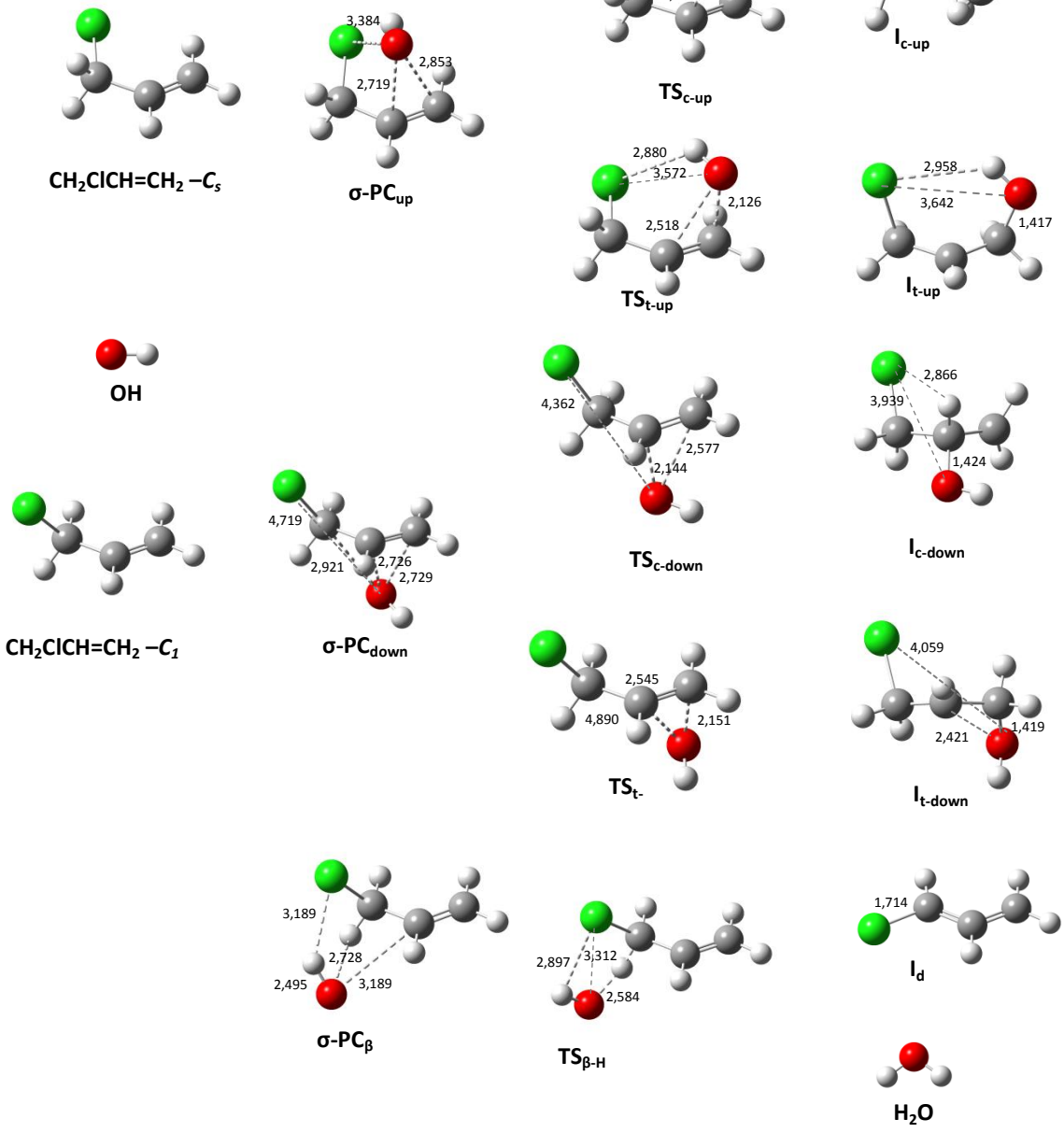

Figure 3. Geometries of the stationary points found along the studied reaction pathways

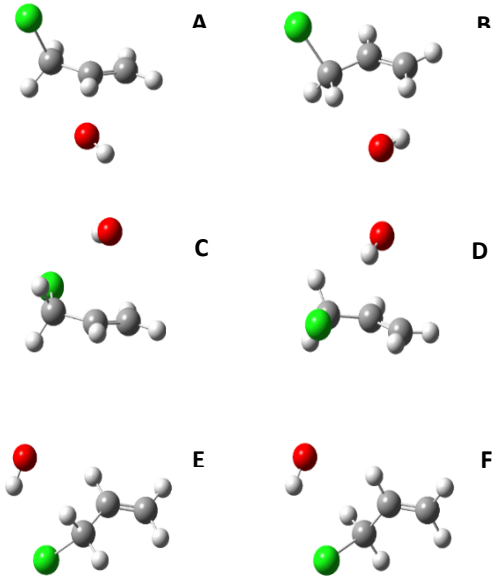

Figure 4: Geometries obtained for the 2 stereoisomers of σ-PC_{down} (a-b), σ-PC_{up} (b-c) and σ - PC_{β} (e-f).

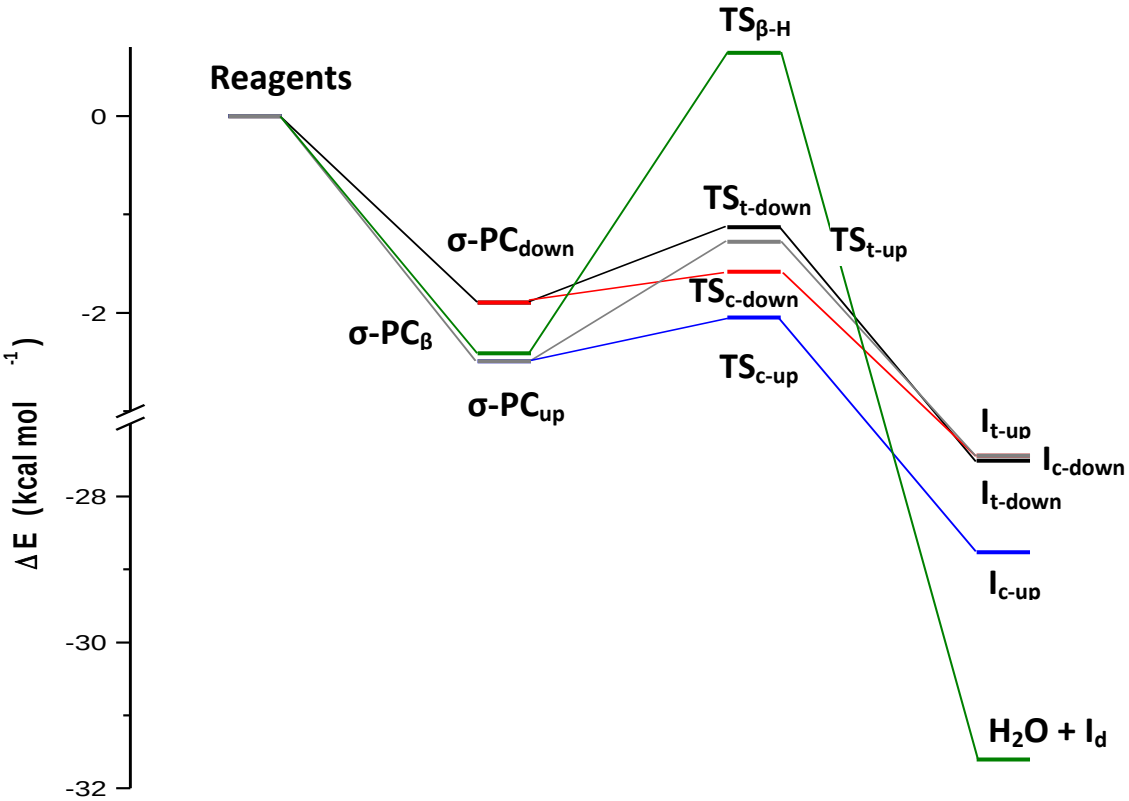

Figure 5. Relative energy of the stationary points of the studied reaction pathways.